3rd CIRP Conference on Surface Integrity (CIRP CSI)

The influence of alloy chemistry on the cutting performance and deformation kinetics of titanium alloys during turning

Pete Crawforth*, Chris M Taylor, Sam Turner

Advanced Manufacturing Research Centre with Boeing, Advanced Manufacturing Park, Catcliffe, Rotherham, S60 5TZ, UK

* Corresponding author. Tel.: +44-0114-222-6673. *E-mail address:* p.crawforth@amrc.co.uk

Abstract

Machining trials were undertaken to study how alloy chemistry influences the relative cutting performance and resulting subsurface deformation for a series of commercially available titanium alloys of increasing β content. Using an experimental orthogonal machining operation, this project focuses on studying what factors influence how efficiently a cutting insert can become embedded into a workpiece and how these factors further influence the overall cutting process.

1. Introduction

There is a growing body of evidence that demonstrates how subsurface deformation generated during machining is sensitive to both the microstructure of the workpiece and machining parameters, such as cutting speed and feed rate [1-3]. There is also awareness that the imparted deformation can be regarded as 'damage', since its presence has been shown to be deleterious [4]. This investigation studies the primary factors that influence the forces during machining and subsequent microstructural deformation. Cutting forces are important to machinists, as the level of force can affect vibration limits, imparted residual stresses and tool fracture.

2. Nomenclature

K_c	Tangential cutting coefficients
K_f	Feed cutting coefficients
P_1	Cutting edge coefficients
P_2	Feed edge coefficients

3. Experimental process

3.1. Materials tested

In order to investigate the role of alloy chemistry on cutting force coefficients (CFCs) and machining induced deformation, the following commercial titanium alloys were supplied by Timet Ltd, as shown in Table 1. The range of α+β titanium alloys demonstrates an increase in β stability, with Ti-6242 being a near α and Ti-5553 being a near β titanium alloy. This can be illustrated using the alloys' molybdenum equivalency number, [5] this factor is an indicator of quantity of β stabilising elements and as such is indicative of how much β phase is contained within the material's microstructure.

Table 1 Generic compositions, room temperature ultimate tensile strength (UTS) and molybdenum equivalency for the experimental alloys

Material	Composition wt.%	Mo Eqv.	UTS MPa
Ti-6242	Al-6.5, Sn-2.25, Zr-4.5, Mo-6.5, Fe-0.15, O-0.15, C-0.04, N-0.04	2.4	1004
Ti-54M ELI	Al-4.7, V-4, Mo-0.68, Fe-0.53, O-0.09, C-0.007	4.7	850
Ti-575	Al-5.3, V-7.7, Fe-0.2, Si-0.5, O-0.2, C-0.05	5.7	1180
Ti-17	Al-5, Sn-2, Zr-2, Mo-4, Cr-4, O-0.16, C-0.05, N-0.13	9.0	1172
Ti-5553	Al-5.12, V-4.7, Mo-4.7, Fe-0.31, Fe-2.77, Si-0.05, O-0.1282, C-0.009, N-0.0055	12.1	1159

The relationship between the resultant cutting forces and the machining feed rate have been commonly used as a measure of a material's machining performance, with

researchers adopting the Oxley model, which can be used to gain cutting force coefficients (CFCs) from the plotted data.

For this investigation each of the alloys were provided by Timet Ltd in billet form, measuring >150 mm in diameter and >200 mm in length. The material specimens were supplied in the as-forged condition, whereby the billet has been allowed to cool slowly following hot working. Following this cool, the material has not been subjected to any further thermomechanical processing or heat treatments.

3.2. Machining trials

In order to benchmark a material's relative cutting force performance, the following experimental procedure was used to capture machining cutting force coefficients (CFCs). The experimental machining arrangement employs an orthogonal cutting condition, comprising of a 4 mm thick ring cut into the face of each of the titanium billets, with an outer diameter approximately equal to the original diameter of the supplied workpiece. During each cutting trial the cutting insert is brought into contact with the ring such that the direction of feed is parallel to the billet axis, and such that the cutting edge is perpendicular to the direction of feed. In order to obtain the materials' CFCs, the average steady state forces are obtained for a series of variable feed rate trials, with each cut undertaken using a fixed surface speed (40 m.min^{-1}) and depth of cut (equal to ring thickness, 4 mm). For each successive trial, the feed rate is increased in 0.05 mm.rev^{-1} increments between 0.1 mm.rev^{-1} and 0.25 mm.rev^{-1}, with individual feed rate trials conducted with a maximum of 3 repeats. A new cutting edge was used for each test. Throughout the trials the force feedback response was recorded using a Kistler 9121 dynamometer that held the tool holder. The output signals were processed through a Kistler 5070 amplifier and the data was recorded using at an acquisition rate of 20 kHz. Table 2 details the tools used during average force measurement investigations. In addition to the standard CFC trial inserts, two additional insert types were chosen in order to investigate the role of edge preparation on the resulting cutting forces and their subsequent effect on microstructural deformation.

Table 2 Tooling required for orthogonal cutting force trials

Operation	Insert		Tool Holder
CFC Average force measurement	TCMT 16 T3 08 KM H13A **Edge radius ~35 μm**		
Cutting trial for additional microstructural assessment	TCMT 16 T3 04-KF H13A **Edge radius ~40 μm**		STGCL-2020K-16
Cutting trial for additional microstructural assessment	TCMW 16 T3 08 H13A **Edge radius ~20 μm**		

For all operations; Hocut 795B, 5% concentration, delivered at 13 l.min^{-1}

An Alicona InfiniteFocus SL high-resolution microscope was used to assess the edge radius of each insert. Figure 1a shows a typical point cloud image, with Figure 1b illustrating the corresponding edge profile and average edge radius determined using a circle best-fit function.
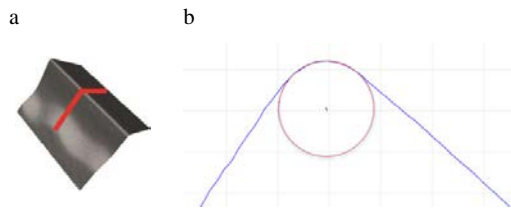

Figure 1 (a) Alicona InfiniteFocus 3D point cloud, (b) application of a profile scan and circle best-fit profile.

4. Results and discussion

4.1. Cutting force coefficients

The data in Figure 2 and Table 3 show the resulting cutting force coefficients for both the cutting and feed components of force. The cutting force (K_c) and feed force (K_f) coefficients corresponds to the gradient of the linear relationship. The cutting (P_1) and feed (P_2) edge coefficients are determined by extrapolating the linear relationship to the y-intercept.
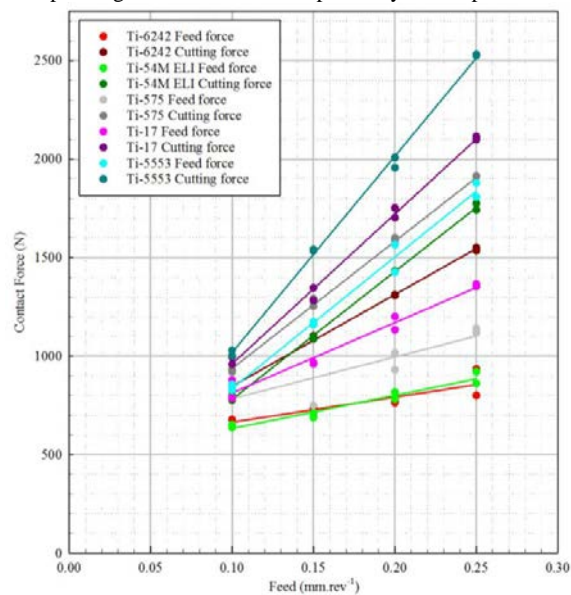

Figure 2 CFC plots for the cutting and feed components.

Table 3 Material CFC components (units shown to 3 significant figures).

Material	K_c	K_f	P_1	P_2
Ti - 6242	4660	1270	380	538
Ti - 54M ELI	6490	1680	130	465
Ti - 574	6460	2110	290	573
Ti - 17	7610	3570	200	456
Ti - 5553	9970	6670	22.0	170

The CFC data illustrates how as the molybdenum equivalency of the alloys is increased; the force coefficients (K_c and K_f) also increase. This suggests that there is a potential dependency with alloy chemistry and, in turn, the material mechanical properties. This observation may align with the attributed increase in room temperature UTS with increasing molybdenum equivalency, as previously shown in Table 1. The edge coefficients (P_1 and P_2) do not however seem to display a sensitivity to alloy chemistry.

Using a cutting force 'offset method' as detailed by Crawforth [6], which utilises cutting force data obtained during the 'bedding-in' period, the CFCs can be determined for each insert. The plots shown in Figure 3 illustrate the sensitivity of the edge coefficients to edge radius. The resulting cutting edge coefficient (P_1) demonstrates little sensitivity to the edge radius of the insert, however in the feed force edge coefficient (P_2) a relationship is evident, with large edge radius inserts requiring an increased amount of force to be embedded.
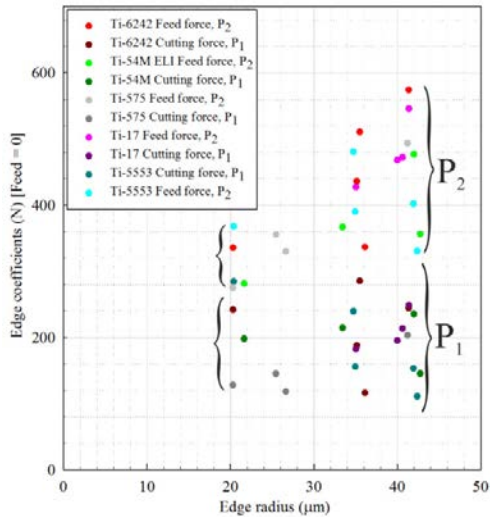

Figure 3 Plots showing the cutting (P_1) and feed force (P_2) edge coefficients.

4.2. Microstructural analysis

Following the turning operation metallurgical samples were taken. In order to normalise any potential variation in crystallographic texture, each sample was obtained from comparable axial and circumferential locations [6]. (Normalised referring to each sample being obtained from comparable locations on a single material type. There will however be an unavoidable uncertainty when comparing material types due variability in the materials thermomechanical history). The polarized light micrographs shown in Figure 4 illustrate the high level of plastic strain being accommodated by the subsurface microstructure. The uppermost region of material beneath the machined surface exhibits a swept type microstructure, typically associated with the passing of the tool parallel to the cutting direction. This region of displaced material gives a clear visual representation of the amount of imparted plastic strain. For the more α-stabilised alloys, Ti-6242, Ti-54M ELI and Ti-575, each displays evidence of mechanically induced twinning. As the micrographs show, Ti-54M ELI showed the highest propensity for twinning.

The plot given in Figure 5 shows a clear discernible difference in the maximum depth to which the severe grain deformation could be observed. Here it was observed that machining with inserts of larger edge radius resulted in deeper deformation. This is an interesting observation and has been attributed to the differences in the expected strain field within the workpiece surrounding the cutting edge. Therefore, for an insert of increased edge radius there will be an increased contact area, which in turn is expected to cause a deeper distribution of stress within the workpiece.
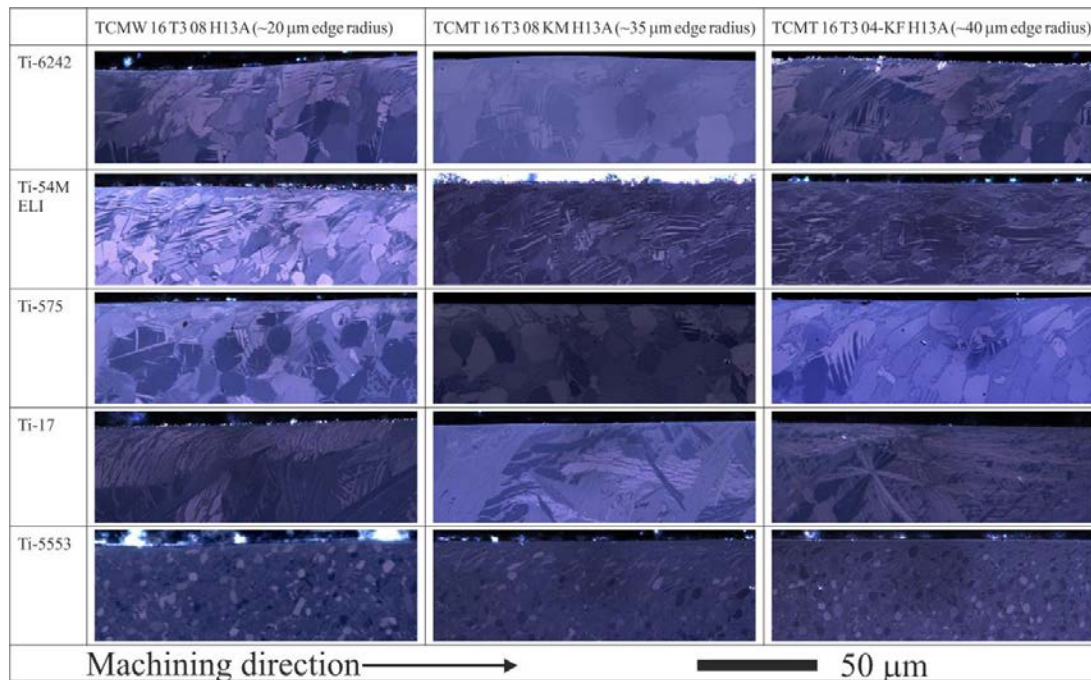

Figure 4 Cross sectional polarized light micrographs of the sub-surface microstructural deformation following machining with inserts of edge radius ~20 μm, ~35 μm, and ~40 μm. Each machined at 40m.min⁻¹ and a feed rate of 0.2 mm.rev⁻¹.
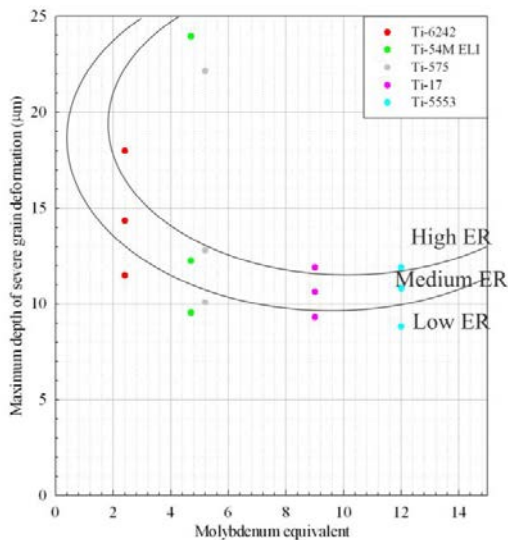
Figure 5 The resulting maximum depth of severe grain deformation as a function of molybdenum equivalency.

The plots given in Figure 6 show the resulting maximum depth of induced twinning and the resulting twin density at 20 μm depth. Both Ti-6242 and Ti-54M ELI saw an increase in the maximum depth to which twinning was observed with an increase in insert edge radius from 35 to 40 μm. Ti-575 however recorded a reduction; this has been attributed to not only the alloy's apparent reduced propensity to induced twinning but also further regional variations in the materials texture, which may otherwise be unfavourably crystalographically orientated for twinning to occur.
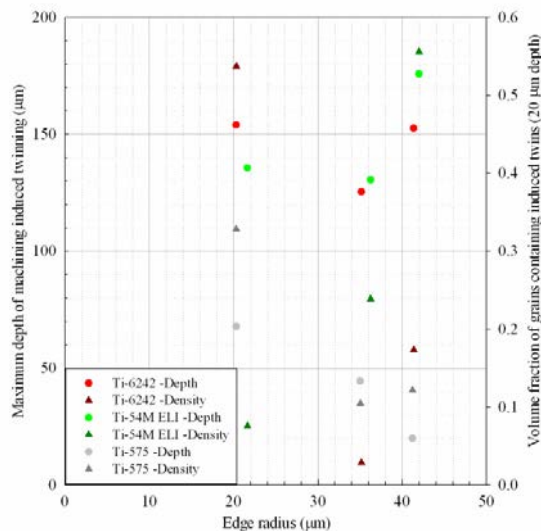

Figure 6 Depth of twinning as a function of insert edge radius and alloy type

For the twin containing alloys, each show an increase in the twin densities when machined with 35 to 40 μm edge radius inserts. As Figure 6 illustrates, the results for the 20 μm inserts do not fit this trend. This has been attributed to excessive vibrations that appear to have been exacerbated by the insert's basic geometry, which does not possess a chip breaker.

5. Conclusions

In order to investigate the role of alloy chemistry on cutting force coefficients and machining induced deformation, the following commercial titanium alloys were supplied by Timet Ltd; Ti-6242, Ti-54M ELI, Ti-575, Ti-17 and Ti-5553. These α+β titanium alloys demonstrate an increase in β stability, with Ti-6242 being a near α and Ti-5553 being a near β titanium alloy. In order to benchmark a material's relative cutting force performance, an experimental procedure was used to capture machining CFCs. In addition to the standard CFC trials, two additional insert types were chosen in order to investigate the role of edge preparation on the resulting cutting forces and their subsequent effect on microstructural deformation.

The acquired cutting force coefficient plots illustrated how as the molybdenum equivalency of the alloys is increased, the respective cutting force (Kc) and feed force (Kf) coefficients also increase. This suggested that there could be a potential dependency on CFCs with alloy chemistry and, in turn, the material properties.

Examination of the near surface microstructure was carried out using polarized light microscopy; this revealed the presence of a highly deformed region containing severely deformed grains as well as twins. The severity of the deformation showed sensitivity to the alloy composition and insert edge radius. For high molybdenum equivalent alloys the severity of the sub-surface deformation lessened. The induced deformation also showed sensitivity to the edge radius of the insert used, with a larger radius resulting in deformation occurring to a greater depth. The results also demonstrated how the edge radius of an insert had a more significant influence on the resulting deformation for alloys with a molybdenum equivalency less than 6. Therefore, for these alloys in order to mitigate the amount of induced severe deformation it is suggested to preferentially opt for inserts that possess a low edge radius.

References

[1] Jawahir, I.S., Brinksmeier, E., M'Saoubi, R., Aspinwall, D.K., Outeiro, J.C., Meyer, D., Umbrello, D., Jayal, A.D., "Surface Integrity in Material Removal Processes: Recent Advances" CIRP Annals, 60/2/2011, P.603
[2] Crawforth, P., Wynne, B.P., Turner, S., Jackson, M., "Subsurface deformation during precision turning of a near-alpha titanium alloy". Scripta Materialia, 67(10), 842–845.
[3] Axinte, D.A., Andrews, P., Li, W., Gindy, N., Withers, P.J., Childs, T.H.C., "Turning of advanced Ni based alloys obtained via powder metallurgy route" CIRP Annals, 55/1/2006, P.117
[4] Maier, H., Teteruk, R., Christ, H.J., "Modeling thermomechanical fatigue life of high Temperature Titanium Alloy IMI 834," Metall. Mater. Trans. A, vol. 31, no. 2, pp. 431–444, 2000.
[5] Lutjering, G., Williams, J. C., "Fundamental Aspects" in Titanium, 2nd ed. Springer, 2007.
[6] Crawforth, P., "Towards a Micromechanistic Understanding of Imparted Subsurface Deformation During Machining of Titanium Alloys," The University of Sheffield, (Thesis) 2014.